Ce-valence instability in the antiferromagnetic and ferromagnetic host series $CeMn_2(Si_{1-x}Ge_x)_2$

G. Liang and M. Croft
Department of Physics and Astronomy, Rutgers University, Piscataway, New Jersey 08855-0849
(Received 6 September 1988; revised manuscript received 13 February 1989)

Lattice, magnetic, transport, and Ce L_3-edge spectroscopic measurements on the $CeMn_2(Si_{1-x}Ge_x)_2$ system are presented. Mixed-valent and low-energy-scale Kondo effects are shown to thrive within the Mn-moment antiferromagnetically ordered phase in this series. The Mn-moment ferromagnetically ordered phase in this series, on the other hand, exhibits nearly to pure Ce^{3+} hard-moment-type behavior. Ce crystalline-electric-field, Kondo, and coherent Kondo effects occurring in this series are discussed.

I. INTRODUCTION

The phenomena of rare-earth valence mixing, the Kondo effect, and heavy-fermion behavior address the quenching of local (often $4f$) moment magnetism through low-energy-scale interaction with itinerant-band electronic states.[1-3] A multitude of studies have documented such phenomena in rare-earth (especially Ce) materials formed by compounding with elements from wide ranges of the Periodic Table. Very little work, however, has been carried out on systems in which the low-energy-scale ($T<100$ K) $4f$ moment quenching coexists with high-energy-scale ($T>300$ K) internal $3d$ magnetism. $CeMn_2Si_2$ has recently been shown to be such a system in which Ce-valence mixing effects occur at temperatures well below the Mn antiferromagnetic (AF) ordering temperature ($T_N=376$ K).[4] Cr substitution for Mn in this system dramatically lowers the energy scale for Ce-moment quenching, and induces a Kondo–heavy-fermion Ce state with sufficient substitution.[5] This alloy study demonstrated the ability of quite low-energy-scale Ce spin-flip scattering to thrive within an AF host phase. However, the incoherent character of Ce scattering and the suppression of the Mn-AF order by the Cr substitution were limiting factors in this study. In this paper, we study the $CeMn_2(Si_{1-x}Ge_x)_2$ system where the Mn magnetic ordering temperature remains high (about 310 K) while the Ce spin-fluctuation temperature scale appears to be driven down rapidly with increasing x. Moreover, the preservation of low-temperature coherence, the appearance of sharp crystalline-electric-field effects and a transition to Mn-moment ferromagnetism all combine to make this alloy system unique.

II. EXPERIMENTAL

Polycrystalline samples were prepared by standard arc furnace techniques. Except the one with $x=0.1$, all of the casted resistivity sample rods were annealed in a quartz tube at 800 °C for 5 d, then cooled down to room temperature. The resistivity $\rho(T)$ measurements were performed by a standard four-probe dc technique in a temperature range of 1.7–300 K. The magnetic moment $M(T)$ measurements were made with a superconducting quantum interference device (SQUID) magnetometer in a magnetic field up to 50 kOe and a temperature range of 2–400 K. The samples for $M(T)$ measurement were taken from the same resistivity sample rods after the electric resistivity $\rho(T)$ measurements were done. The L_3 measurement and Ce L_3-valence determination method has been described elsewhere.[6,7] X-ray powder-diffraction measurements on all samples showed single phase of body-centered tetragonal crystal structure of the $ThCr_2Si_2$ type.

III. RESULTS AND DISCUSSION

A. L_3-XAS introduction

L_3-edge x-ray absorption spectroscopy (XAS) has been proved to be a very valuable tool in determining the valence in the mixed-valence field.[6-10] The large number of unoccupied $5d$ orbitals in rare-earth atoms produces (via $2p\rightarrow 5d$ transition) a prominent peak (the so-called L_3 white line) just above the L_3 absorption edge. In addition, an arctangent-type step function feature, due to $2p_{3/2}\rightarrow$continuum transitions, occurs at the L_3 edge. In the past, the rapid time scale for the XAS measurement compared to the intervalence tunneling time has been involved to explain the "snapshot" character of the L_3 XAS spectrum.

The principle of the Ce valence determination by L_3-edge XAS can be motivated on a more microscopic level in the following way. In some Ce compounds there is a strong hybridization between the $4f$ level and the conduction-band states, putting the Ce compounds into a mixture of the pure $|f^0\rangle$ and $|f^1\rangle$ states (the mixing of the $|f^2\rangle$ configuration is normally very small because of the large Coulomb interaction between f electrons). If the mixing of $|f^0\rangle$ is quite large, say, more than 10%, then we say that the Ce compound is in the mixed-valence regime. One can, in general, denote the wave function of the initial state (the state before absorbing a photon) of the Ce compound by $\psi_i=a_0|f^0\rangle+a_1|f^1\rangle$. In the absorption, a $2p_{3/2}$ electron is kicked out by the photon into the $5d$ conduction band, leaving behind a $2p_{3/2}$

hole in the Ce atom. Due to the strong Coulomb interaction C [$\approx 7-10$ eV (Ref. 11)] between the $2p_{3/2}$ hole and $4f$ electron, the energy level of the final state $\psi_{\text{fin},1}(\sim|f^1\rangle)$ is positioned about 7–10 eV below the energy level of the final states $\psi_{\text{fin},0}(\sim|f^0\rangle)$. A simple matrix model calculations can show that the mixing of $|f^0\rangle$ in $\psi_{\text{fin},1}$ and $|f^1\rangle$ in $\psi_{\text{fin},0}$ is on the order of 0.01 or less. Here V ($\approx 0.01-0.1$ eV) is the hybridization strength.[12] Thus, the transitions of the initial state ψ_i of the Ce compound into the final states $\psi_{\text{fin},1}(\sim|f^1\rangle)$ and $\psi_{\text{fin},0}(\sim|f^0\rangle)$ yield an L_3 edge, which is a superposition of two integral valent (f^0 and f^1) edges separated by $C \approx 7-10$ eV. The intensities of the f^0 peak (Ce^{4+} peak) and the f^1 peak (Ce^{3+} peak) should be proportional to $|a_0|^2$ and $|a_1|^2$, respectively, with an error of 0.01 or less. Thus, the weight of each valence configuration (f^0 or f^1) in the initial valence state is evaluated by determining the spectral weight of the two integral valent edge features (or peak features) required to model the spectrum and the Ce L_3-valence value v_3 can be obtained. One can see that it is the many-body final-state effect that makes the Ce-valence measurement possible through L_3 XAS technique (with about 1% error). Discussions of similar final-state effects in XAS measurements have been given by Fuggle *et al.*[11] and Gunnarson *et al.*[11]

In Fig. 1 (top), we illustrate these ideas by showing the separate Ce^{3+} and Ce^{4+} components used to model the Ce L_3 spectrum of $CeMn_2Si_2$ ($T=300$ K) (pictured in the same figure). The details of the fitting procedure have been discussed elsewhere.[7] The derived L_3-valence value (v_3) for this material is $v_3=3.12$. Whether the L_3 valence is in fact the absolute valence for Ce compounds is, at present, an outstanding question. However, in many score of Ce systems, a one-to-one correspondence has been established between the Ce volume collapse (associated with Ce valence mixing) and the Ce L_3-valence change. The spirit in which we use the L_3-valence values, therefore, is to identify changes in the Ce valence state.

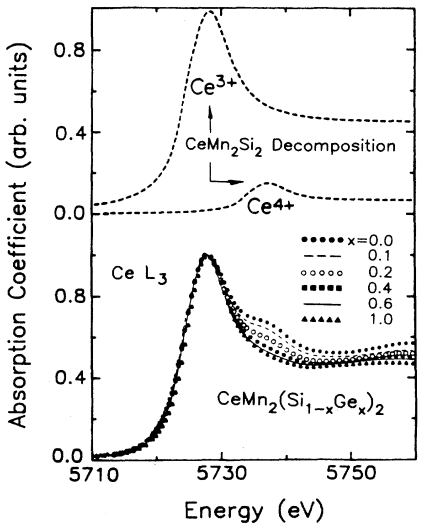

FIG. 1. Ce L_3 absorption spectra of $CeMn_2(Si_{1-x}Ge_x)_2$ compounds superimposed to compair intensity in Ce peak region, all normalized to the Ce^{3+} peak.

We display the experimental Ce L_3 spectra superimposed and normalized to the first (Ce^{3+} related) peak. With this normalization-superpositions procedure, a spectra with a higher v_3 value will lie naturally above a spectrum with a lower v_3 value in the energy range of the second (Ce^{4+} related) peak. In this way, a fitting procedure independent illustration of the spectrum evolution associated with Ce valence changes can be seen.

B. L_3 XAS and lattice parameter results

Shown in Fig. 1 (bottom) is the L_3 x-ray absorption spectroscopy for $CeMn_2(Si_{1-x}Ge_x)_2$, with all spectra normalized to the low-energy (Ce^{3+}) spectral peak. A higher energy (Ce^{4+}) peak is clearly evident at $x=0.0$. This Ce^{4+} feature gradually weakens with increasing x and finally disappears for $x>0.6$. The Ce L_3 valence, v_3, obtained by our fitting procedure[6,7] is plotted versus x and shown in Fig. 2 (bottom). At $x=0$, v_3 is 3.12, indicating that $CeMn_2Si_2$ is a mixed-valent (MV) compound (for comparison $v_3=3.15$ for $CePd_3$). With x increasing, v_3 rapidly decreases, and beyond $x=0.6$, it is nearly trivalent with value $v_3 \leq 3.01$.

In previous work we have proposed a MV-Kondo regime borderline nominally in the Ce L_3-valence value range $3.08 \leq v_3 \leq 3.10$ for the CeT_2Si_2 series with T being a $3d$ element (see Ref. 4). This empirical crossover region corresponds here a narrow range between $x=0$ and 0.1, where the v_3 is changing (with x) most rapidly. We wish

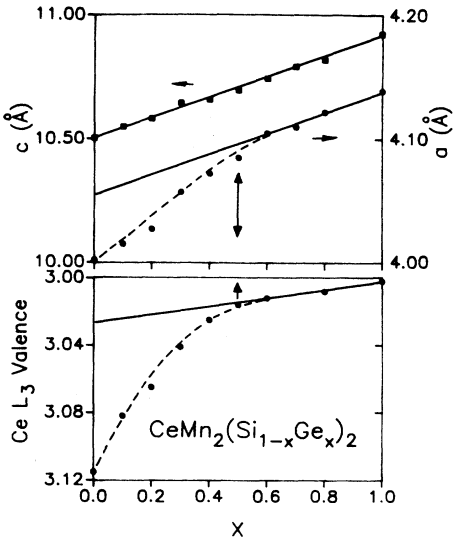

FIG. 2. (Top) The a and c lattice parameters of the $CeMn_2(Si_{1-x}Ge_x)_2$ system. Note the linear variations (vs x) of a and c are indicated by straight (solid) lines. The dashed lines are guides to the eye highlighting the nonlinear compression in the a parameter for $x<0.5$. (Bottom) The Ce L_3-valence variation (v_3) for this system. Note the nonlinear increase in v_3 for $x<0.5$ highlighted by the dashed line. Note also the linear, close to the Ce^{3+} behavior of v_3 in the $x>0.5$ range.

to note that the v_3 continues to change in the Kondo regime $x \geq 0.1$. The notion that the Ce valence would continue to vary a certain amount in the Kondo regime as the spin-fluctuation energy scale is varied has been stressed in a number of recent theoretical works.[13] The division between MV and Kondo regimes is also somewhat arbitrary since the conventional underlying Anderson model Hamiltonian can be used (with varying parameters) to continuously link the two regimes. A better sense of the crossover between these two regimes will emerge from our resistivity results discussed below.

The a and c lattice parameters of this series are also plotted in Fig. 2 (top). It is typical of 1:2:2 compounds that the c parameter is insensitive to rare-earth sublattice atomic radius variations and hence the Vergard's law type behavior for c for all x in this system is not unexpected. The a parameter in 1:2:2 compounds, on the other hand, is known to respond to rare-earth radius changes.[14,15] Accordingly, it should be noted that in the $x \geq 0.6$ range, where v_3 is nearly constant, the a parameter shows a linear variation; in the $x < 0.6$ range, where v_3 shows a nonlinear increase, the a parameter shows an analogous nonlinear compression. Thus, the valence variation evidenced by the L_3 results is excellently supported by the lattice parameter variations.

C. Magnetic moment and magnetism

1. Phase diagram

Shown in Fig. 3 is the thermal dependence of the magnetization $M(H,T)$ in various fields and susceptibility $\chi(T)$ for selected samples in the $CeMn_2(Si_{1-x}Ge_x)_2$ system. Our magnetic measurements confirm and extend the work of Siek *et al.*[16] Our magnetic measurements support the division of the T-x phase diagram of this system into the following regions (originally proposed by Siek *et al.*).[16]

(1) $0.0 \leq x \leq 0.3$. In this region, the Mn atoms exhibit antiferromagnetic order and thus a sharp peak at T_N is evidenced in the $M(T)$ and $\chi(T)$ curves [see Figs. 3(a) and 3(b)].[17] The amount alignment presumably remains along the c axis as in the $x=0.0$ material.[17]

(2) $0.3 \leq x \leq 0.55$. In this region the system passes through three magnetic regimes with decreasing temperature. First, the high-temperature paramagnetic (PM) phase transforms to a ferromagnetic (FM) phase at T_c. Then, at a temperature T_1 ($T_1 < T_c$), a nonlinear decrease from the typical FM $M(T)$ behavior indicates the development of an AF component in the internal magnetization. Since the response to the external field retains a large FM component for $T < T_1$, the designation of intermediate (IM) phase has been given to this region. Finally, we identify a temperature $T_2 < T_1$ at which one exits the IM phase and enters a low-temperature AF phase. T_2 has been chosen as the point of maximum slope in the $M(T)$ curve of $x=0.4$ and as the shoulder in the $M(T)$ curve of $x=0.5$.

(3) $0.55 < x \leq 1.0$. In this region, a normal PM-FM transition occurs at $T_c \approx 310$ K [see Fig. 3(c) for $x=0.7$ example].

If the empirically defined temperatures T_1 and T_2 bounding the IM are in fact second-order phase transitions, then the multicritical (MC) point, where the T_N, T_c, T_1, and T_2 lines meet, is a tetracritical point.[18–21] If the IM is a two-phase coexistence of AF and FM regions, then the T_N and T_c lines meet at a bicritical point with

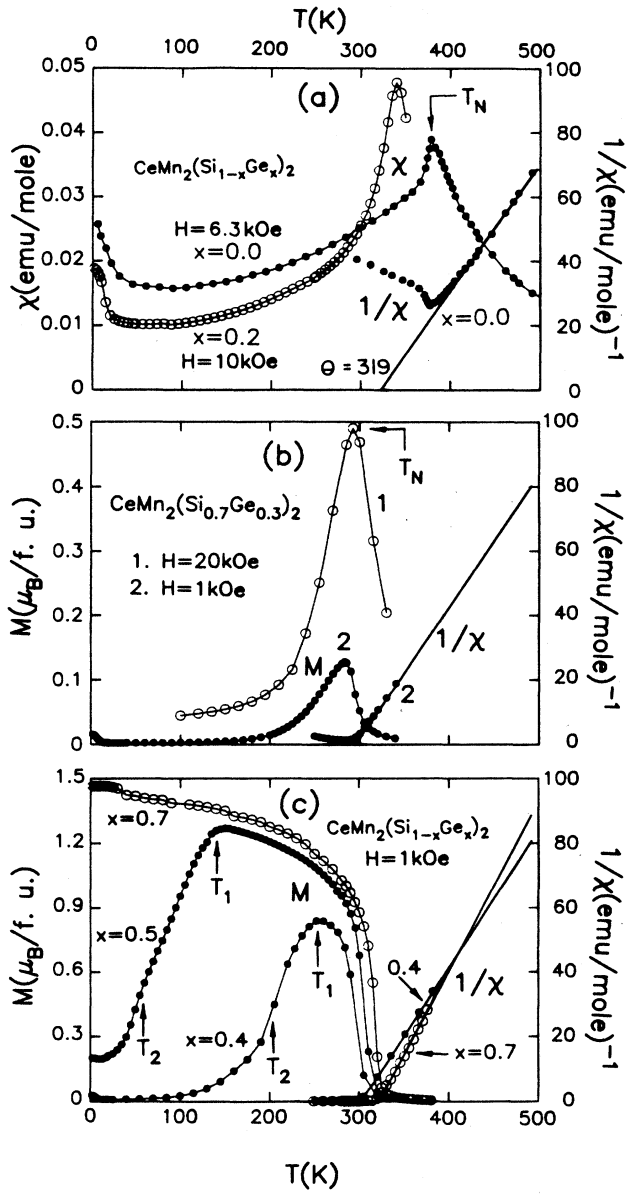

FIG. 3. Temperature dependence of the magnetic susceptibility $\chi(T)$ and magnetic moment $M(T)$ of the $CeMn_2(Si_{1-x}Ge_x)_2$ series under different external field H. Note the decreasing of T_N with x increasing for $x \leq 0.3$ in (a) and (b). T_1 and T_2 are defined as the transition temperatures from ferromagnetic to intermediate phase and from intermediate to antiferromagnetic phase, respectively (see the text). The $1/\chi$ data were plotted against T for sample with $x=0.0$, 0.3, 0.4, and 0.7. The straight, solid lines through the $1/\chi$ data points are the fit $1/\chi=(T-\Theta_p)/C$ to the data points in the paramagnetism region, where C and Θ_p are the Curie constant and paramagnetic Curie-Weiss temperature, respectively.

the AF↔*FM* transition being first order.[18–21] In view of the very continuous deviation of the $M(T)$ curve from FM behavior upon cooling below T_1, we currently favor the former of these choices. In either case, the downward curvature of the $T_N(x)$ and $T_c(x)$ lines approaching $x=0.3$ is typical of such multicritical points.[18–21] Clearly single-crystal magnetic and neutron-scattering measurements are needed to clarify the IM region of this phase diagram.

2. *Transition temperature and effective moments*

In Table I, T_N, T_c, T_1, and T_2 are listed together with the paramagnetic Curie-Weiss temperature Θ_p, effective moment μ_{eff}, and the resistivity minimum temperature T_{min} (discussed below). The Θ_p and μ_{eff} values were obtained by fitting the data to a Curie-Weiss law $\chi=C/(T-\Theta_p)$ on the high-temperature (paramagnetic) side of $1/\chi(T)$ curves. It should be noted that the data points above T_N extend only about 100 K above T_N. However, from our previous work on $CeMn_2Si_2$,[4] it is clear that extending the Curie-Weiss fit to 400 K above T_N changes Θ and μ_{eff} values by only about 3%. Several features can be seen from Table I and the phase diagram in Fig. 4. First, the magnetic ordering temperature is depressed 15% between the Si and Ge end points. Since the magnetic ordering energy is governed basically by the in-plane Mn interactions, this effect is presumably due to the weakening of these interactions accompanying the volume expansion. Second, both the AF and FM transition temperatures are depressed anomalously near the critical concentration ($x\approx 0.3$) for AF→FM crossover. This is presumably due to frustration induced reduction in the internal field, which accompanies the competing AF and FM fluctuations. As noted above, such a downward cusp in the ordering temperature is common in systems which exhibit a AF→FM crossover with a bicritical or tetracritical point.[18–21] Third, similar to $Ce(Mn_xCr_{1-x})_2Si_2$ series (see Ref. 5) μ_{eff} of the Mn in this series is much smaller than the 5.9 μ_B of the $Mn^{2+}(3d^5)$ ion and tends to be reduced with increasing Ge substitution. Fourth (as we will discuss at greater length below), the closeness of the resistivity minimum T_{min} and T_1 ($T_{\text{min}}<T_1$ always) for $0.3\le x\le 0.5$ indicates that the Ce spin-flip scattering is freed up when an AF component to the Mn magnetization develops.[5]

For some of the samples, a weak upturn of $M(H,T)$ was observed at low temperatures (i.e., below 40 K) which tends to saturate below 2 K). The amplitude of the $M(H,T)$ enhancement due this upturn is very small, i.e., about 0.014 μ_B per formula unit (f.u.) in the AF phase and about 0.025 μ_B/f.u. in the FM phase. We believe that this upturn is due to a small amount of the impurities $CeSi_x$ ($1.7\le x\le 2.0$) (Ref. 22) for which T_c lies in the $T\approx 10$ K range ($x=1.7$ and 1.8). Such $CeSi_x$ inclusions could be caused by Mn mass loss in the sample preparation process since Mn is quite volatile. The concentration is less than 1% of the Ce atoms by saturation moment estimate. No evidence for Ce atoms ordering was observed for the $CeMn_2(Si_xGe_{1-x})_2$ system.

3. *Higher magnetic-field response*

In an AF material, which exhibits a crossover to FM order upon alloying and must always be FM or saturated PM for sufficiently high fields, the higher magnetic-field response is an interesting question. Accordingly, we plot in Fig. 5 the M versus H isotherms for selected samples and temperatures in this system.

In the FM regime, we note the magnetization curves rise (with increasing field) extremely rapidly in the low-field ($H<1$ kOe) region (i.e., see Fig. 5, the $x=0.6$ and 0.5 curves at $T=40$ and 150 K, respectively). Domain and anisotropy effects mask the spontaneous magnetization in these measurements. The lack of saturation in the $H>10$ kG range is presumably due to magnetocrystalline anisotropy effects in our polycrystalline sample. That is, while these crystallites, with their easy axis parallel to the

TABLE I. Magnetic data for $CeMn_2(Si_{1-x}Ge_x)_2$ compounds determined from the tempeature-dependence measurements of magnetic moment. AF is antiferromagnetic ordering; FM is ferromagnetic ordering; IM is the intermediate phase between antiferromagnetism and ferromagnetism; T_c is the Curie ordering temperature; T_N is the Néel temperature; T_1 is the transition temperature from the FM→IM phase; T_2 is the transition temperature from the IM→AF phase; T_{min} is the resistivity minimum temperature; Θ_p is the paramagnetic-Curie-Weiss temperature; μ_{eff} is the effective moment; H is the applied external field during moment $M(T)$ measurements.

X	T_N (K)	T_c (K)	T_1 (K)	T_2 (K)	T_{min} (K)	Θ_p (K)	μ_{eff} (μ_B/Mn)	H (kOe)	Magnetic phase
0.0	376					319	3.28	6.3	AF
0.2	340					294	3.07	10.0	AF
0.3	291				242	288	3.08	20.0	AF
0.3	281				242	296	3.04	1.0	AF
0.4		305	252	204	237	302	3.07	1.0	IM
0.5		310	150	75	147	312	2.81	1.0	IM
0.6		320				320	2.48	0.2	FM
0.7		320				322	2.81	1.0	FM
1.0		316[a]				316[a]	2.76[a]	6.0[a]	FM

[a]The results of Narasimhan and Szytula *et al.* for $CeMn_2Ge_2$ are also represented (Ref. 28).

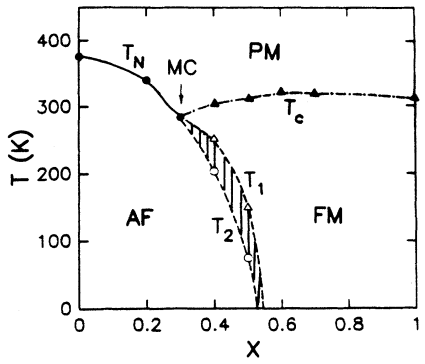

FIG. 4. The temperature vs concentrations phase diagram of the $CeMn_2(Si_{1-x}Ge_x)_2$ system as determined by the magnetic moment $M(T)$ measurements. The AF, FM, and PM labels refer to the antiferromagnetic, ferromagnetic, and paramagnetic phases for the Mn sublattice order. T_N and T_c represent the Mn-AF (Néel) and Mn-FM (Curie) ordering temperature. The T_1 and T_2 dashed curves are defined in text. MC represents the multicritical point of the magnetic phase transition (see the text). The dashed region represents the Mn FM-AF crossover region, or the intermediate phase region in the text.

applied field, saturate quickly the other crystallities require very large external fields to pull their magnetization away from the easy direction. For example, the magnetization at 50 kOe (for the $x=0.6$ sample) is about 2.5 μ_B/f.u., which is 17% smaller than a saturation moment $gS\mu_B=3.0$ μ_B/f.u. (or 2.1 μ_B/Mn) expected on the basis of the high temperature $\mu_{\text{eff}}\approx 2.8$ μ_B/Mn listed in Table I (note $g=2.23$ as in $CeMn_2Si_2$ has been used here).[5]

Deep within the AF phase the Mn moments are locked into the large internal field and the magnetization response to the external field is extremely small. For example, see the $T=100$ K, $x=0.3$ $M(H,T)$ curve where the magnetization at 50 kOe is roughly 0.1 μ_B/f.u. A single $M(H,T)$ point (open triangle) for the $x=0.3$ sample at $H=20$ kOe and $T\approx T_N=291$ K is included in Fig. 5. This point indicates a 0.5 μ_B/f.u. response of the sample to a 20 kOe field at this temperature. This ferromagnetically enhanced large response is due to the fact that the underlying interactions, which set the transition energy scale, are ferromagnetic. Also, the crossover to FM initial ordering occurs very close to $x=0.3$ so that upon ordering this sample is, in fact, on the verge of a FM state.

At low fields the sample with $x=0.4$ at $T=150$ K is within what we have called the AF phase. However, it is just below the temperature T_2, which we have associated with the exit from the intermediate phase. We note in Fig. 5 that the magnetization curve for this sample shows a greatly enhanced response (0.7 μ_B/f.u. at 50 kOe) compared to that in the true AF phase. The continuous evolution toward ferromagnetism, which occurs in the IM with increasing T, is illustrated by the magnetization of the same $x=0.4$ at $T=230$ K (in the IM) in Fig. 5. By 50 kOe, this curve has attained a value essentially as large as seen in the FM region, however, the lower-field response is more spread out. Presumably, a continuous field induced reduction of the AF order parameter is involved here.

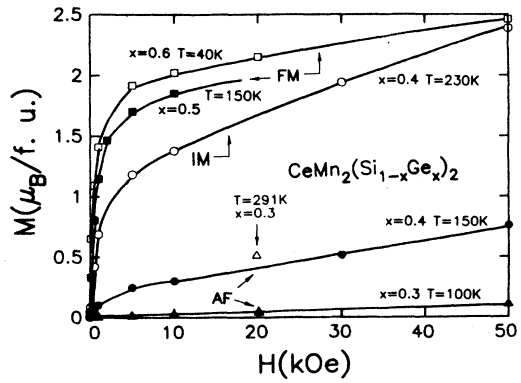

FIG. 5. External magnetic-field dependence of the magnetic moment $M(H)$ for several samples at different temperatures. The AF, FM, and IM labels refer to the antiferromagnetic, ferromagnetic, and intermediate phases for the Mn sublattice order. The single point (open triangle) at $H=20$ kOe is for the $x=0.3$ sample at $T\approx T_N=291$ K [see Fig. 3(b)].

D. Resistivity results

1. x dependence

A number of competing effects combine to give a wealth of different structures in the temperature and concentration dependences of the resistivity in this alloy series. Before discussing the more complicated thermal variation, we will address first the somewhat simpler resistivity variation across the series at high ($T=270$ K) and low ($T=2$ K) temperature (see Fig. 6). Both of these $\rho(x)$ curves exhibit similar structure, i.e., a pronounced

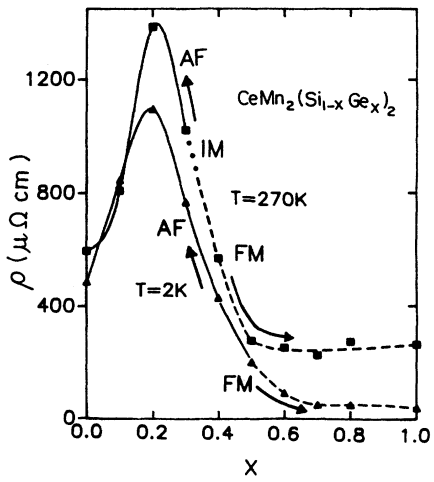

FIG. 6. The resistivity, ρ, of polycrystalline samples in the $CeMn_2(Si_{1-x}Ge_x)_2$ system at 270 and 2 K. The lines connecting the experimental points are solid, dotted, and dashed in the antiferromagnetic (AF), intermediate (IM), and ferromagnetic (FM) phases of the series, respectively. Here the phase diagram results, i.e., Fig. 4, have been used.

increase from $x=0.0$ to a maximum at $x=0.2$, followed by large drop to a low and almost concentration-independent value above $x=0.5$. This sort of behavior has been observed a number of times before in a system which can be driven (by alloying or pressure) from an MV to Kondo regime[23,24] [e.g., $Ce(Pd,Ag)_3$ or $Ce(Rh,Pd)_3B$]. Specifically, the behavior is the overall resistivity in the Kondo regime rises rapidly as the MV regime is approached (in this case this is as x varies from 1.0 toward 0.1), the resistivity peaks (at $x=0.2$ here) quite close to (but before) the MV regime is reached, and the resistivity drops strongly as the MV regime is more closely approached and entered (i.e., below $x<1.0$ here).

We wish to emphasize that this seemingly typical MV→Kondo evolution (with increasing x) in the resistivity is occurring within a magnetically ordered compound. The antiferromagnetic, ferromagnetic, and "intermediate phase" regions of order in this system have been shown in Fig. 4. The AF, IM, and FM regions (at 270 and 2 K) have been indicated on the $\rho(x)$ curves in Fig. 6 by using different types of lines connecting the data points. The sharp drop of resistivity for $T=270$ K in the IM and FM region ($0.3\leq x\leq 0.5$) and the nearly concentration independent resistivity for both $T=270$ and 2 K in the FM region (above $x=0.5$) may be related to the influence of ferromagnetism on the Ce sites.

2. *Temperature dependence of resistivity*

The temperature dependence of the resistivity in the $CeMn_2(Si,Ge)_2$ system involves the interplay of not only Kondo–MV effects, crystalline-electric-field (CEF) effects, and narrow-band coherence effects, but also of competing antiferromagnetic, ferromagnetic, and "intermediate" magnetic phases. In order to help clarify the situation, we have drawn the resistivity curves (see Fig. 7) which lie in the antiferromagnetically ordered phase using a solid line; those which lie in the ferromagnetically ordered phase by a dashed line; and those which lie in a intermediate phase by a dotted line. Here the locus of the AF, FM, and IM phases have been estimated by the phase diagram shown in Fig. 4. This phase diagram is reproduced in Fig. 8 (dashed lines) of this text also. We will now partition and discuss these resistivity curves in several classes.

3. *Mixed-valent range: $x<0.1$*

The $x=0.0$ materials, as has been noted previously, shows a resistivity typical of well-ordered mixed-valent material (like $CePd_3$, for example).[25] The rapid fall off in $\rho(T)$ below the maximum (labeled A') at $T=73$ K is typical of the onset of coherent scattering between the MV-Ce sites. The immunity of the Ce-MV behavior to the antiferromagnetically ordered Mn sublattice stems apparently from the fact that the Ce sites lie (by symmetry) at nodes in the internal Ruderman-Kittel-Kasuya-Yosida (RKKY) field.[4,5]

4. *CEF-Kondo range: $0.1\leq x\leq 0.5$*

One of the first rules of thumb developed to differentiate between MV and Kondo regime systems was

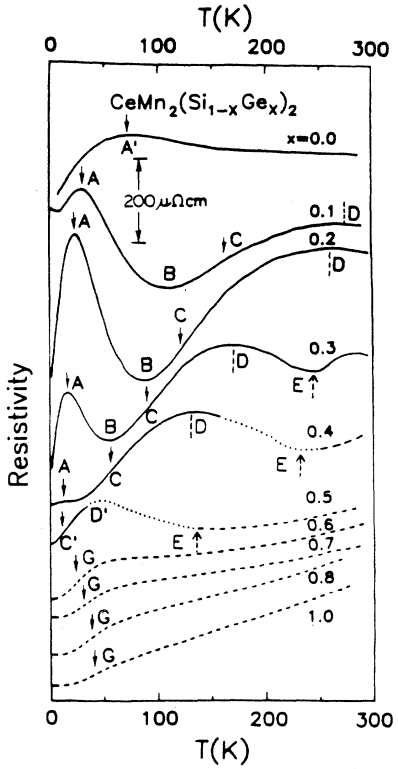

FIG. 7. The resistivity vs temperature for the $CeMn_2(Si_{1-x}Ge_x)_2$ system. The curves are solid, dotted, and dashed in the antiferromagnetic, intermediate, and ferromagnetic phases, respectively. Again, the phase diagram Fig. 4 was used to assign the magnetic phases. See the text for a discussion of the various resistivity features labeled by letters in the figure.

that the Kondo regime materials often exhibited CEF splitting effects but MV materials invariably did not. The rationale for this was that the spin-fluctuation or charge-fluctuation temperature in the MV materials was high enough to wash out the sharp CEF splitting and CEF states were admixed by such f-orbital fluctuations. Comparison of our $x=0.0$ to our $0.1\leq x\leq 0.4$ $\rho(T)$ results provides a dramatic example of this rule of thumb. In this second region $0.1\leq x\leq 0.4$, the $\rho(T)$ curves show the double maximum structure typical of HF-Kondo lattice systems (like $CeCu_2Si_2$), which exhibit a CEF modified Kondo scattering combined with a low-temperature coherence effect. The minimum at $T<20$ K for $x=0.1$ samples is attributed to this sample being somewhat more disordered (not annealed).

For clarity we labeled some of the more prominent features in the resistivity curves with letters. The sharp low-temperature maximum (occurring between 10 and 31 K in the $0.0\leq x\leq 0.4$ region) is labeled A and the minimum which occurs at somewhat higher temperatures, is labeled B. The rise in the resistivity between B and A is attributed to incoherent Kondon scattering from the Ce-CEF ground state. The fall in the resistivity at temperatures below A is associated with the onset of coherent narrow-band behavior among the Ce sites. The

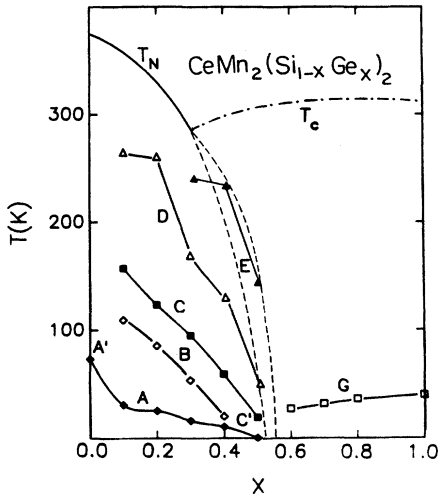

FIG. 8. The loci in the T-x plane of the resistivity features (A–E and G) labeled in Fig. 7. Also shown is the magnetic phase diagram Fig. 4. The dashed-dotted and solid lines are, respectively, the FM-T_c and AF-T_N lines from Fig. 4. The dashed lines indicate the crossover between AF and FM order.

maximum in the MV, $x=0.0$ sample was labeled A' since, in terms of marking the onset of coherence, it is related to the A features in the Kondo regime.

At temperatures (T) above the B (lower-temperature local resistivity minimum) features the resistivity rises substantially and the halfway-inflection point in this rise has been labeled C. The second (higher-temperature) maximum has been labeled D. Finally (for the $0.1 \leq x \leq 0.4$ region), the highest-temperature local resistivity minimum is labeled E. The drop in the resistivity (with decreasing T) from D to C to B is attributed to the "freezing out" of the Kondo scattering from an excited CEF level (or levels). The rise in the resistivity (with decreasing T) from E to D is associated with the Kondo scattering, when the excited CEF level is populated. As noted above, such a CEF modified Kondo lattice behavior has been seen a number of times previously.[26,27] However, it has never been observed in a host which is magnetically ordered over the entire range of the effect (as is the case here).

A point we want to emphasize regarding this CEF-Kondo regime ($0.1 \leq x \leq 0.4$) is that the Ce spin-fluctuation energy scale almost certainly becomes quite low in this range. The variations in the temperature of the low-temperature maximum feature A (T_A), have been used in Kondo–heavy-fermion systems in the past to qualitatively estimate variations in the spin-fluctuation temperatures (T_{SF}). T_A is expected to track T_{SF}. In our system T_A is 30, 25, and 16 K in the $x=0.1$, 0.2, and 0.3 samples, respectively. This low-energy scale spin-fluctuation behavior is especially remarkable in view of the ordering temperature of the Mn sublattice always being greater than 310 K.[28] The degredation of the low-temperature maximum (A) in the $x=0.4$ sample suggests that the magnetic environment (or defects in it) may be disrupting the low-energy scale spin fluctuations.

The loci (in the $T-x$ plane) of the features A, B, C, D, and E are shown in Fig. 8 along with the magnetic phase diagram shown in Fig. 4. The results in Fig. 8 motivate a number of observations. Firstly, the termination of the CEF-Kondo-related feature lines A, B, C, and D for $x<0.1$ emphasizes the disappearance of the resolvable CEF effects in the MV $0 \leq x \leq 0.1$ range. Secondly, the MV regime maximum A' lies sharply up from the Kondo regime extrapolation of the A peaks toward $x=0.0$. This is consistent with the rapid rise in the spin-fluctuation temperature typically observed upon entering the MV state. Thirdly, perhaps the most dramatic effect illustrated by Fig. 8 is the constant decrease in the temperature of all of the Kondo and CEF-related features (A–C) as the ferromagnetic phase is approached (i.e., for x increasing toward $x=0.5$).

Fourthly, we note that the temperature of the highest-temperature resistivity minimum feature E (T_E) tracks the broader of the AF-FM intermediate phase. Before returning to the CEF-Kondo discussion (below), we wish to discuss this point. The highest-temperature resistivity minimum (E) qualitatively identifies where the Kondo scattering becomes important. In the $x=0.3$, 0.4, and 0.5 samples E is correlated with the exit from the ferromagnetic phase and impending entrance into the AF+FM mixed phase upon cooling. In extensive studies on the $Ce(Mn, Fe)_2Si_2$ and $Ce(Mn,Cr)_2Si_2$ series, we have shown that this E (resistivity minimum) feature correlated excellently with the onset of the AF phase.[5] Moreover, through studies on similar AF $ThMn_2Si_2$ alloys, we have shown that the resistivity rise in the AF phase in these Ce compounds is not associated with the Mn magnetic scattering.[5] Moreover, the locking of the Mn moments into a well-established internal field would also argue against any Mn spin-fluctuation contribution to the resistivity. Thus in all of these studies, we find that the entrance or impending entrance of the compounds into the antiferromagnetic phase appears to free up the Ce atoms to exhibit low-energy-scale Kondo-MV interactions with the conduction electrons. Conversely, the paramagnetic phase (as seen in our previous studies[5]) or ferromagnetic phase (as seen below) in these systems appears to exhibit a quenching effect on the Ce-Kondo-MV phenomena.

Returning to the CEF-Kondo discussion, we note that both the resistivity results and the plots of the feature temperatures in Fig. 8 appear at first glance to suggest that a decrease in the CEF splitting may occur with increasing x. The evidence on this matter is the decrease in the temperature difference between the two maxima A and D from near a 235 K at $x=0.1$ to about 120 K at $x=0.4$. Since the maximum D occurs when an excited CEF state begins to freeze out, this would appear to support a decrease in the CEF splitting. For $CeCu_2Si_2$, the first excited CEF level is about 140 K[29] not unlike the splitting that may be present in the $x=0.4$ sample of this series. The second excited CEF level in $CeCu_2Si_2$ is near 364 K.[29] If the CEF structure of the $CeMn_2(Si_{1-x}Ge_x)_2$ is similar to that of $CeCu_2Si_2$, the above effect could be caused by the following scenario. At $x=0.1$, where the spin-fluctuation temperature is high, the two excited CEF levels could be strongly mixed and the maximum D could

reflect scattering from the combined excited levels. It should be noted that within the Cornut-Coqblin model of the CEF-Kondo effect, the spin-fluctuation temperature drops dramatically as excited CEF level depopulation occurs.[26] This could permit the excited CEF levels to be strongly mixed at high temperatures (when T_{SF} was large) but allow the CEF ground state to be well resolved at low temperature (when T_{SF} is much smaller.) At higher x values where the spin-fluctuation temperature is lower the two excited CEF levels could be decoupled so that the maximum would reflect the lower excited level only. Thus, within this proposal the "apparent" decrease in the CEF arises from a crossover (with increasing x) from scattering dominated by the combined excited CEF levels at $x=0.1$ to scattering dominated by the lowest excited CEF at $x=0.4$. Since we would not anticipate strong changes in the CEF splitting, we favor an explanation, of the sort proposed above, to explain the resistivity data. Clearly, inelastic neutron-scattering studies would be of great value here.

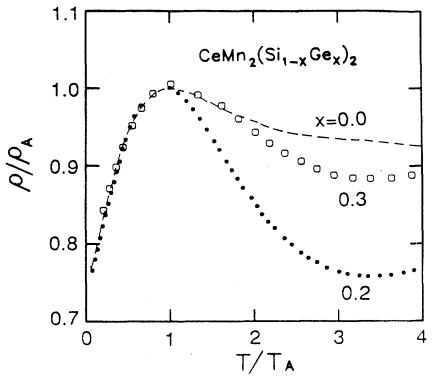

FIG. 9. The scaled low-temperature resistivities of the $x=0.0$. 0.2, and 0.3 samples of the $CeMn_2(Si_{1-x}Ge_x)_2$ system as a function of T/T_A and ρ/ρ_A. Here T_A and ρ_A are the temperature and resistivity of the low-temperature maximum (labeled A and A' in Fig. 4). The rounded universal behavior of the scaled resistivity supports the common coherency interpretation of the low-temperature drop in resistivity.

5. *Coherence in $0 \leq x \leq 0.4$ range*

We would like to discuss the variation of the low-temperature coherent effect in our series. The development of "coherence" is one of the most intriguing characteristics of HF and MV materials.[23] We have noted that we associate the resistivity drop at temperatures below $T_{A'}$ and T_A with the onset of such coherent intersite Ce scattering. We further associated the depression of T_A with increasing x with the depression of the spin-fluctuation temperature and the "coherency temperature" [i.e., $T_{coh} \approx T_{max} 2/(2J+1)$ from Lawrence *et al.*].[30] Here T_{coh} is a measure of the energy scale of the intersite coupling in the coherent state.

In order to support the notion that the sharp drop below T_A, for $0.1 \leq x \leq 0.3$, is due to coherent scattering rather than other effects like magnetic order of the Ce sites, we plotted ρ/ρ_{max} versus T/T_{max} for $x=0.0$, 0.2, 0.3 (shown in Fig. 9). (Here $T_{max}=T_A$ and $\rho_{max}=\rho_A$.) We did not choose the $x=0.1$ sample because it was not annealed. The good scaling behavior observed for $T/T_{max}<1$ in Fig. 9 is consistent with the coherency interpretation for these resistivities.[30] This scaling behavior suggests that a single characteristic energy may be used in spite of the presence of a strong $3d$ AF RKKY field and further that this energy scale decreases by nearly a factor of 5 with increasing x. For $T/T_{max}>1$, the scaling breaks down because of the influence of the CEF.

Similar scaling behavior was also observed for the $Ce(Cu_xNi_{1-x})_2Si_2$ series[31] and $CeCu_2Si_2$ under very high external pressure.[27] However, by comparison, this scaling behavior is not found for $CeCu_2X_2$ with X=Si and Ge even for $T/T_m<1$ (see Fig. 10). This is because of the rather sharp drop of ρ below T_{max} in $CeCu_2Ge_2$, as is typical in many magnetically ordering Ce systems.

Since no single impurity Kondo behavior was observed in our $CeMn_2(Si,Ge)_2$ resistivity results, we conclude that the disorder of Si-Ge sublattice has little influence on the coherency effect. This apparent preservation of low-temperature coherency in the $CeMn_2(Si_{1-x}Ge_x)_2$ system stands in contrast to the single-impurity-type Kondo scattering observed in the $Ce(Mn_{1-x}Cr_x)_2Si_2$ system.[5] Thus, it would appear that Si sublattice substitution is, in this sense, less locally violent than Mn sublattice substitution.

6. *$x=0.5$ intermediate regime*

We elect to discuss the $x=0.5$ sample separately since it lies in the "intermediate" portion of the phase diagram shown in Fig. 4, where the precise magnetic state is somewhat uncertain. The local resistivity minimum E is presumably associated with the impending exit from the ferromagnetic phase with decreasing T and the onset of Kondo scattering (similar to the E feature in the $x \leq 0.4$ range). The lower-temperature maximum and subsequent falloff appear more closely related to features in the $x \geq 0.6$ range discussed below.

7. *$x=0.6<x \leq 1.0$ ferromagnetic phase*

The $\rho(T)$ curves in this range are all dominated by a phononlike positive slope. A small drop occurs in all of these curves in the 20–40 K range and is labeled at the center of the drop as feature G in Fig. 7. Above this drop subtraction of a true phonon background would yield a weak Kondo-like upturn in the resistivity in the 50–100 K range. This last weak upturn is most apparent in the $x=0.6$ sample data. The locus of the G feature points are included in Fig. 6. Thus, the resistivity curves in this range show little, if any, evidence for Ce spin-fluctuation effects.

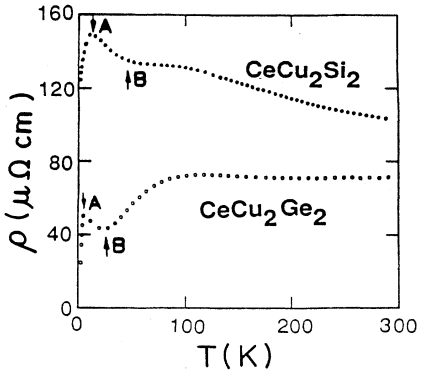

FIG. 10. The resistivities of $CeCu_2Si_2$ and $CeCu_2Ge_2$. Note in particular the CEF related structure in both curves in the 50–100 K range and the resistivity rise due to Kondo scattering from the CEF ground state below 25 K in both curves. The rounded decrease in resistivity below the 10 K maximum for $CeCu_2Si_2$ due to coherent Kondo scattering should be contrasted with the sharp drop in $CeCu_2Ge_2$, presumably due to the onset of magnetic order.

IV. SUMMARY AND CONCLUSIONS

The $CeMn_2(Si_{1-x}Ge_x)_2$ system has shown evidence of a MV-to-Kondo regime crossover (with increasing x) while remaining deep within an ordered Mn-moment phase of the AF type. That is, while the AF ordering energy remains greater than 300 K the Ce-MV-Kondo spin-fluctuation energy scale appears to vary roughly from $T_{SF} \approx 100$ K to $T_{SF} < 10$ K with increasing x. Moreover, a sharp CEF structure and intersite coherent Kondo scattering appear to operate relatively freely despite the Mn magnetic order and Si↔Ge substitution. At higher Ge concentrations, FM Mn-moment order accompanies the onset of near Ce^{3+} stable moment behavior.

This work motivates several questions. One such question is just how low an energy scale and how subtle a Ce moment quenching behavior can be achieved within a robustly ordered host. Another is how the RKKY oscillation in the conduction electron spin density interact with the Ce moment Kondo compensation cloud. A third question is whether the AF→FM change in the Mn ordering is a product of the Ce-valence and/or moment change or vice versa. Finally, an intriguing question arises as to whether external magnetic fields of sufficient strength could drive an AF to a saturated moment FM on the Mn sublattice and whether this change would then couple to a large Ce-valence-moment change.

ACKNOWLEDGMENTS

We would like to than K. V. Ramanujachary, E. A. Hayri, and E. Wang for their assistance in magnetic moment measurement.

[1]J. M. Lawrence, P. S. Riseborough, and R. D. Parks, Rep. Prog. Phys. **44**, 1 (1981).
[2]G. R. Stewart, Rev. Mod. Phys. **56**, 755 (1984).
[3]See Koln Conference on Valence Instabilities, Koln, 1984 [J. Magn. Magn. Mater. **47&48**, 1 (1985)], and references therein.
[4]G. Liang, I. Perez, D. DiMarzio, M. Croft, D. C. Johnston, N. Anbalagan, and T. Mihalisin, Phys. Rev. B **37**, 5970 (1988); G. Liang, M. Croft, R. Neifeld, and B. Qi, J. Appl. Phys. **61**, 3818 (1987).
[5]G. Liang, M. Croft, D. C. Johnston, N. Anbalagan, and T. Mihalisin, Phys. Rev. B **38**, 5302 (1988).
[6]R. A. Neifeld, M. Croft, T. Mihalisin, C. U. Segre, M. Magigan, M. S. Torikachvili, M. B. Maple, and L. E. DeLong, Phys. Rev. B **32**, 6928 (1985).
[7]M. Croft, R. Neifeld, C. U. Segre, S. Raan, and R. D. Parks, Phys. Rev. B **30**, 4164 (1984).
[8]K. P. Bauchspiess, W. Boksch, E. Holland-Moritz, H. Launois, R. Pott, and D. Wohllenben, Phys. Rev. B **32**, 417 (1985).
[9]R. D. Parkks, S. Raaen, M. L. den Boer, V. Murgai, and T. Mihalisin, Phys. Rev. B **28**, 3556 (1983).
[10]P. Weidner, K. Keulerz, R. Lohe, B. Roden, J. Rohler, B. Wittershagen, and D. Wohlleben, J. Magn. Magn. Mater. **47&48**, 75 (1985).
[11]O. Gunnarsson and K. Schonhammer, Phys. Rev. B **28**, 4315 (1983); J. C. Fuggle, F. U. Hillebrecht, Z. Zolnierek, R. Lasser, Ch. Freiburg, O. Gunnarsson, and K. Schonhammer, *ibid.* **27**, 7330 (1983); J. C. Fuggle, F. U. Hillebrecht, J.-M. Estva, R. C. Karnatak, O. Gunnarsson, and K. Schonhammer, *ibid.* B **27**, 4637 (1983).
[12]For example, see M. Croft, E. Kemly, and C. U. Segre, Solid State Commun. **44**, 1025 (1982).
[13]N. E. Bickers, D. L. Cox, and J. W. Wilkins, Phys. Rev. B **36**, 2036 (1987); P. Schlottman, Z. Phys. B, **56**, 127 (1984).
[14]E. Kemly, M. Croft, V. Murgai, L. C. Gupta, C. Godard, R. D. Parks, and C. U. Segre, J. Magn. Magn. Mater. **47&48**, 403 (1985).
[15]E. V. Sampathkumaran, R. Vijayaraghavan, K. V. Gopalakrishnan, R. G. Pilley, H. G. Devare, L. C. Gupta, Ben Post, and R. D. Parks, in *Valence Fluctuations in Solids,* edited by L. M. Falicov, W. Hanke, and M. B. Maple (North-Holland, New York, 1981), p. 93; E. V. Sampathkumaran, G. Kalkowski, C. Laubschat, G. Kaindl, M. Domke, G. Schmiester, and G. Wortmann, J. Magn. Magn. Mater. **47&48**, 212 (1985).
[16]S. Siek and A. Szytula, J. Phys. **40**, 162 (1979).
[17]S. Siek, A. Szytula, and J. Leciejewicz, Phys. Status Solidi A **46**, K101 (1978).
[18]Michael E. Fisher and David R. Nelson, Phys. Rev. Lett. **24**, 1350 (1974).
[19]A. D. Bruce and A. Aharony, Phys. Rev. B **11**, 478 (1975).
[20]Ch. Wissel, Phys. Status Solidi B **51**, 669 (1972).
[21]G. Eggarter and T. P. Eggarter, Phys. Rev. B **15**, 2804 (1977).
[22]H. Yashima and T. Satoh, Solid State Commun. **41**, 723 (1982).
[23]J. Ward, J. E. Crow, and T. Mihalisin, in *Crystalline Electric Fields and Structural Effects in f-Electron Systems,* edited by Jack E. Crow, Robert P. Guertin, and Ted. W. Mihalisin (Plenum, New York, 1980), p. 333.

[24]I. Perez, M. Croft, G. Liang, J. B. Zhou, S. A. Shaheen, and H. Jhans, J. Appl. Phys. **61**, 3180 (1987).
[25]P. Scoboria, J. E. Crow, and T. Mihalisin, J. Appl. Phys. **50**, 1895 (1979).
[26]B. Cornut and B. Coqblin, Phys. Rev. B **5**, 4541 (1972).
[27]S. Horn, M. A. Edwards, J. D. Thompson, and R. D. Parks, J. Magn. Magn. Mater. **52**, 355 (1985).
[28]A. Szytula and I. Szott, Solid State Commun. **40**, 19 (1981); K. S. V. L. Narasihan, V. U. S. Rao, R. L. Bergner, and W. E. Wallace, J. Appl. Phys. **46**, 4957 (1975).
[29]S. Horn, E. Holland-Moritz, M. Loewenhaupt, F. Steglich, H. Scheuer, A. Benoit, and J. Flouguet, Phys. Rev. B **33**, 3171 (1981).
[30]J. M. Lawrence, J. D. Thompson, and Y. Y. Chen, Phys. Rev. Lett. **54**, 2537 (1985).
[31]J. Ray, E. V. Sampathkumaran, and Girish Chandra, Phys. Rev. B **35**, 2095 (1987).